NMR Methods for Studying the Structure and Dynamics of RNA

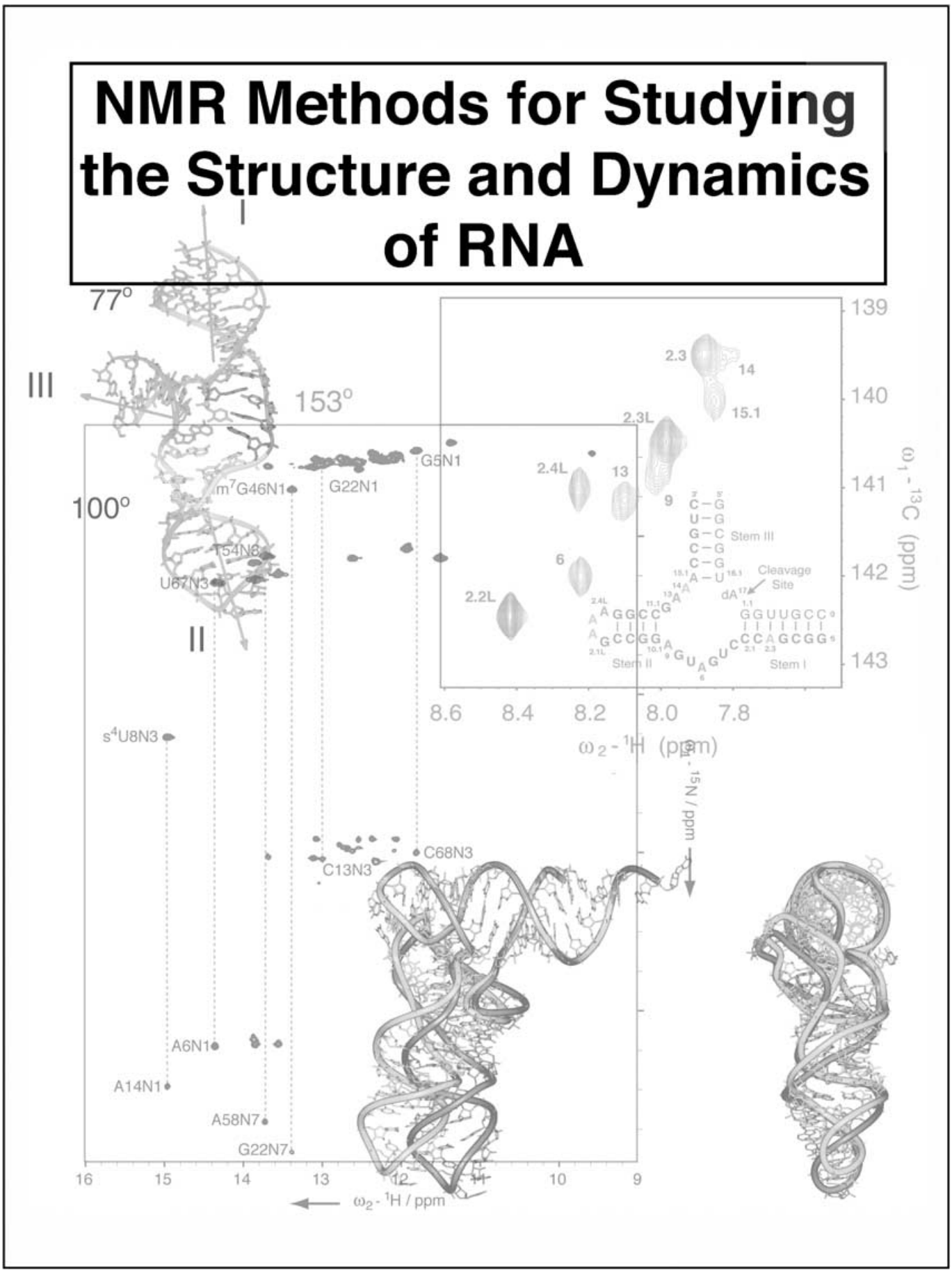

  DOI: 10.1002/cbic.200500123 *ChemBioChem* **2005**, *6*, 1492 – 1505

NMR Methods for Studying the Structure and Dynamics of RNA

Michael P. Latham,[a] Darin J. Brown,[a] Scott A. McCallum,[a, b] and Arthur Pardi*[a]

Proper functioning of RNAs requires the formation of complex three-dimensional structures combined with the ability to rapidly interconvert between multiple functional states. This review covers recent advances in isotope-labeling strategies and NMR experimental approaches that have promise for facilitating solution structure determinations and dynamics studies of biologically active RNAs. Improved methods for the production of isotopically labeled RNAs combined with new multidimensional heteronuclear NMR experiments make it possible to dramatically reduce spectral crowding and simplify resonance assignments for RNAs. Several novel applications of experiments that directly detect hydrogen-bonding interactions are discussed. These studies demonstrate how NMR spectroscopy can be used to distinguish between possible secondary structures and identify mechanisms of ligand binding in RNAs. A variety of recently developed methods for measuring base and sugar residual dipolar couplings are described. NMR residual dipolar coupling techniques provide valuable data for determining the long-range structure and orientation of helical regions in RNAs. A number of studies are also presented where residual dipolar coupling constraints are used to determine the global structure and dynamics of RNAs. NMR relaxation data can be used to probe the dynamics of macromolecules in solution. The power dependence of transverse rotating-frame relaxation rates was used here to study dynamics in the minimal hammerhead ribozyme. Improved methods for isotopically labeling RNAs combined with new types of structural data obtained from a growing repertoire of NMR experiments are facilitating structural and dynamic studies of larger RNAs.

1. Introduction

RNAs have been shown to play important roles in an increasing variety of biological functions, with functions ranging from carrying genetic information to catalysis and regulation. One of the goals of RNA structural biology is to understand how structure and dynamics lead to a specific function of an RNA. Solution NMR spectroscopy represents an important tool for probing the structure and dynamics of RNA and RNA–protein or –ligand interactions. In addition, NMR relaxation methods can be used to obtain dynamic data on timescales ranging from picoseconds to seconds.

In the past few years, the molecule size limit for studying RNA by NMR spectroscopy has increased to beyond 20 kDa. The "divide-and-conquer" approach has long been used to study the structure of smaller pieces of large RNAs. However, general methods were not readily available for combining data from the individual fragments for use in the structure refinement of the larger RNA. Structure determinations of larger RNAs are becoming more routine with recent advances in isotopic-labeling strategies, the ability to directly determine hydrogen-bonding interactions, and methods for obtaining the global structure of a molecule through long-range structural constraints. The measurement of residual dipolar coupling data in partially oriented media is having an enormous impact on the ability to determine the global structures of RNAs, which are often comprised of multiple helical domains. In addition, dynamic information on RNA has become accessible through NMR relaxation data. Some of these developments in NMR studies of RNA have recently been reviewed.[1,2] Thus, we will focus here on methodologies that we expect will significantly impact NMR studies of RNAs: improvements in the acquisition and analysis of residual dipolar coupling data, novel applications of HNN-COSY techniques to probe secondary and tertiary structure, and additional isotopic-labeling strategies that simplify the NMR spectra of larger RNAs. We will also present ^{13}C-relaxation data on the minimal hammerhead ribozyme, demonstrating that the conserved core in this catalytic RNA has multiple residues with microsecond dynamics.

2. Synthesis and Purification of RNA Samples for NMR Studies

One of the challenges in NMR studies of RNA is the requirement for milligram quantities of pure (usually ^{13}C- and/or ^{15}N-labeled) material. Most RNA oligomers for NMR spectroscopy are synthesized by in vitro transcription with a DNA-dependant RNA polymerase, such as T7 RNA polymerase.[3] RNA can also be produced by chemical synthesis and this is a practical option for small, unlabeled RNAs. T7 RNA polymerase requires a guanine residue on the 5′ end of the RNA transcript, and the efficiency of the transcription reaction is very dependant on

[a] *M. P. Latham, D. J. Brown, Dr. S. A. McCallum, Prof. A. Pardi*
Department of Chemistry and Biochemistry
215 UCB, University of Colorado
Boulder, CO 80309-0215 (USA)
Fax: (+1) 303-492-2439
E-mail: arthur.pardi@colorado.edu

[b] *Dr. S. A. McCallum*
Current address:
Genentech Inc., Department of Protein Engineering
S. San Francisco, CA 94080 (USA)

 DOI: 10.1002/cbic.200500123

the specific sequence at the 5′ end of the RNA. In vitro transcription with T7 RNA polymerase often produces inhomogeneous 3′ ends due to the incorporation of one or more extra random-sequence nucleotides by the polymerase.[3] This problem can be reduced by substituting a 2′-methoxyribose sugar for the last two nucleotides (or only the penultimate nucleotide) on the DNA template.[4]

Other methods have also been developed for improving the yield and reducing the heterogeneity of RNA produced by in vitro transcription with T7 RNA polymerase. For poorly transcribing RNAs, the addition of a sequence at the 5′ end that transcribes more efficiently followed by cleavage of this sequence with template-directed RNase-H can substantially improve the large-scale production of RNA.[5] Heterogeneity at the 3′ (and 5′) end(s) of T7 transcripts can be completely overcome by employing cis- or trans-acting ribozyme(s) that specifically cleave the transcript to leave homogeneous length RNA.[6,7] Eliminating the heterogeneity at the 3′ (and if necessary 5′) end of the RNA significantly improves the yield of the desired RNA and enormously simplifies the purification.[8]

NMR structures of small RNAs can be obtained from studies of unlabeled molecules, but the high degree of overlap in RNA spectra means that ^{13}C and/or ^{15}N labeling is required for NMR studies of most larger RNAs. Labeled nucleotides are typically obtained by growing bacteria on a minimal medium with $^{15}NH_4Cl$ as the only nitrogen source and/or ^{13}C-glucose or ^{13}C-methanol as the only carbon source.[9–11] The RNA is extracted and degraded to ribonucleoside monophosphates (rNMPs), which are then purified and enzymatically phosphorylated to ribonucleoside triphosphates (rNTPs). The rNTPs are substrates for T7 RNA polymerase, so this approach yields uniform labeling of the RNA. The four rNMPs can also be separated, converted into their triphosphates, and used to generate RNA oligomers where only a subset of nucleotide types is isotopically labeled.[9,11] It is also possible to overexpress the RNA in *Escherichia coli* from a plasmid and then purify the expressed

Arthur Pardi studied Chemistry at the University of California, San Diego, where he obtained an AB in 1976. He obtained his PhD in Chemistry from the University of California, Berkeley, in 1980 working with I. Tinoco, Jr., where he used biophysical methods to study the thermodynamic and kinetic properties of DNA and RNA duplexes. He then did a postdoctoral fellowship with K. Wüthrich at the ETH, Zürich, where he performed 2D NMR studies of protein and DNA systems. He was appointed Assistant Professor of Chemistry at Rutgers University in New Jersey and moved to the University of Colorado, Boulder, in 1988, where he is currently Professor of Chemistry and Biochemistry. His research focuses on studies of the structure, function, and dynamics of proteins and RNA. His group developed efficient methods for the production of isotopically labeled RNAs and they continue to develop improved NMR methods for determining the structure and dynamics of RNA and protein–RNA systems. Some of the RNA systems that have been studied in his lab include: the hammerhead ribozyme, the leadzyme, tRNAs, RNA aptamers, unusually stable hairpins containing RNA tetraloops, and the iron-responsive RNA. Prof. Pardi's group is presently studying a new RNA-aptamer therapeutic compound, Macugen, which is a potent inhibitor of the angiogenic protein VEGF. NMR structural studies are being performed on the Macugen–VEGF complex. In addition to NMR spectroscopy, Prof. Pardi's group uses biochemical approaches to probe the kinetics of the natural hammerhead ribozyme and they are also employing single-molecule fluorescence spectroscopy techniques to probe the kinetics of folding of RNAs.

Michael Latham studied Chemistry at Hampden-Sydney College in Hampden-Sydney, VA. He obtained his BS in Chemistry in 1999. He is currently a PhD candidate in the group of Prof. Pardi studying the dynamics involved in the activation of the signaling protein kinase Erk2. He is also working on developing improved techniques for NMR spectroscopy studies of RNA.

Darin Brown studied Biomaterials at Case Western Reserve University, Cleveland, OH, and in 1997 obtained his BS degree in Biomedical Engineering. Focusing on the temperature dependence of NMR relaxation experiments in proteins, he obtained his MS degree in Physiology & Biophysics in 2005. He is now working on his PhD degree in Chemistry in the group of Prof. Pardi. His current work involves studying the dynamic transitions of RNA molecules.

Scott McCallum studied Organic Chemistry at the University of New Hampshire, Durham, and obtained his BA in 1991. He then performed his doctoral studies at the University of Virginia, Charlottesville, and the Carnegie Mellon University, Pittsburgh, PA, with G. S. Rule where he determined how structural plasticity is utilized by human GST detoxification enzymes to recognize a broad range of structurally and chemically diverse substrates. He did his postdoctoral work with A. Pardi at the University of Colorado, Boulder. Dr. McCallum is currently in the Department of Protein Engineering at Genentech, Inc., San Francisco, CA.

RNA.[12–14] This substantially reduces the cost and labor for producing isotopically labeled RNAs, but this procedure is not generally applicable because it requires the RNA to be highly resistant to nuclease degradation in *E. coli*.

2.1. Selective isotopic-labeling procedures for RNA

Various isotopic-labeling strategies have been developed to help simplify the resonance assignments and improve the spectral properties of RNA oligomers. Rapid relaxation of the nuclear spins becomes a major problem for larger molecules; therefore, the ability to generate highly deuterated samples has become critical for NMR studies of larger proteins. Several complementary approaches have been developed for obtaining highly deuterated and isotopically labeled RNAs. Nikonowicz and co-workers generated deuterated rNTPs by growing *E. coli* in highly enriched ^2H_2O, with $^{15}NH_4Cl$ as the only nitrogen source and ^{2}H-enriched acetate as the only carbon source.[15] The ^{2}H,^{15}N-labeled RNAs produced with these rNTPs had improved relaxation properties for their exchangeable amino and imino protons. This perdeuteration procedure also improved the signal-to-noise ratio and reduced spectral overlap in NOESY spectra. A further modification of this procedure allowed back protonation of the H8 atoms on purines and H5 atoms on pyrimidines in an otherwise highly deuterated and ^{13}C,^{15}N-labeled RNA sample.[16] The presence of protonated and ^{13}C-labeled bases in a mostly perdeuterated sample should improve the relaxation properties and help simplify resonance assignment of larger RNA systems.

Williamson and co-workers have developed a procedure for producing specifically labeled RNAs by biosynthetically incorporating glucose into rNTPs.[17] By starting from various combinations of uniformly or specifically ^{13}C- and/or ^{2}H-labeled glucose, differential labeling of the proton and carbon atoms in the ribose ring is possible. Since there is currently no inexpensive commercial source for isotopically labeled bases, the bases in these rNTPs are generally not labeled. This method has been used to produce RNAs that are uniformly ^{13}C-labeled in the sugar ring and deuterated at the sugar 3′, 4′, 5′/5″ positions.[17] This gives NMR data on the best-resolved proton signals in the RNA spectrum, that is, the sugar H1′–C1′/H2′–C2′ and the base H2/H8/H5/H6 resonances.

Another selective labeling procedure developed by Hoffman and Holland involves the growth of *E. coli* on either $^{13}CH_3{}^{12}COONa$ or $^{12}CH_3{}^{13}COONa$ as the only carbon source.[18] This approach leads to complementary distributions of ^{13}C atoms in the rNTPs prepared from the *E. coli* (see above). Thus, carbons that are ^{13}C labeled in one growth condition are unlabeled in the other. The RNAs produced with this selective labeling approach have simplified NMR spectra, which facilitates assignments of the sugar and base proton and carbon resonances.

Our group has recently grown *E. coli* by using ^{13}C-formate and ^{12}C-glucose as the only carbon sources. In this combination, ^{13}C-formate is site-specifically incorporated into the C8 position of adenine and guanine bases with $>85\%$ efficiency (see inset in Figure 1), with no evidence of incorporation of the label at other sites. Figure 1 also shows 2D ^{1}H,^{13}C-HSQC of the base region of ^{13}C8-labeled purine valine transfer RNA (tRNA^{Val}). The use of rNTPs from the *E. coli* grown on ^{13}C-formate leads to the production of specifically labeled ^{13}C8-labeled purine RNAs. One valuable application of this specific-labeling technique is the elimination of ^{13}C–^{13}C couplings in the purine ring, which can simplify the analysis of ^{13}C relaxation data (see Section 5).

For large RNAs, it is often helpful to segmentally label individual domains. This is easily accomplished in some systems by synthesizing the RNA in multiple pieces, where the individu-

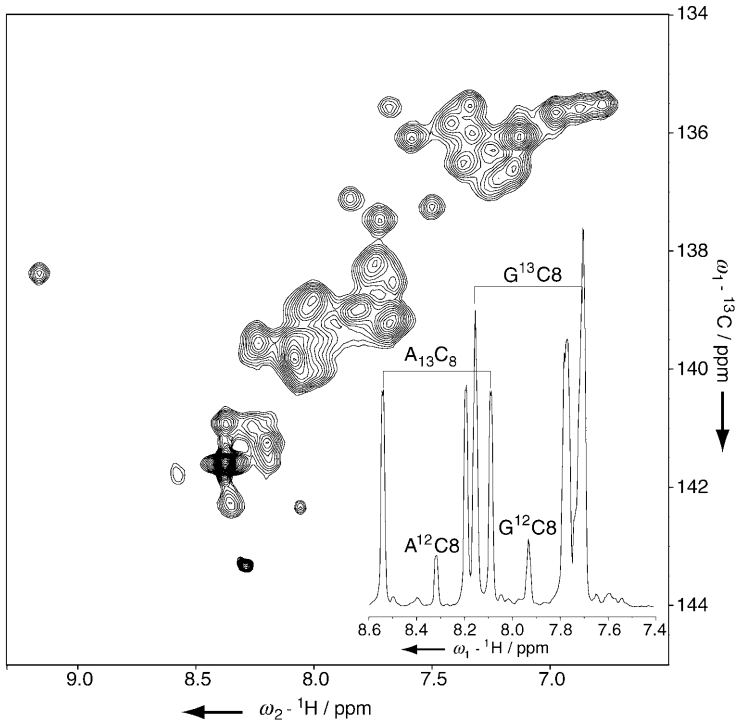

Figure 1. The aromatic region of the 2D ^{1}H,^{13}C-HSQC spectrum of the uniformly ^{15}N-labeled and purine ^{13}C8-labeled native *E. coli* tRNA^{Val}. At least 32 of the expected 39 purine C8–H8 correlations are resolved in this spectrum. The sequence and secondary structure of native *E. coli* tRNA^{Val} is shown as an inset in Figure 4. The aromatic region of a 1D ^{1}H spectrum of ^{13}C8-labeled rNMPs with no ^{13}C decoupling during acquisition is shown in the lower right corner. The H8 resonances coupled to ^{13}C and ^{12}C carbon atoms are highlighted for both G and A. The ratio of the peak intensities was used to estimate that C8 is $\approx 87\%$ ^{13}C labeled. The ^{15}N,^{13}C8-labeled native *E. coli* tRNA^{Val} sample was obtained by overexpression of *E. coli* BL21(DE3) cells containing the pVALT7 plasmid.[12,14] Cells were grown with $^{15}(NH_4)_2SO_4$ (2 g L^{-1}) as the sole nitrogen source and with ^{12}C-glucose (2 g L^{-1}) and 99% ^{13}C-formate (200 mg L^{-1}; Cambridge Isotopes Laboratories, Inc., Andover, MA) as the carbon sources. The purification of tRNA^{Val} was performed as described previously.[14] This yielded a 1.8 mM tRNA^{Val} sample in 10 mM $NaPO_4$ (pH 7.0), 80 mM NaCl, 5 mM $MgCl_2$, 0.1 mM EDTA (pH 8.0), and 10% D_2O. For the ^{13}C8-labeled rNMP sample, complete RNA was digested into monomers and exchanged into D_2O. All NMR experiments were preformed on a 500 MHz Varian INOVA spectrometer equipped with a Varian pulsed-field gradient HCN probe at 25 °C. The 2D ^{1}H,^{13}C HSQC spectra on tRNA^{Val} were collected with 256×1024 (t_1,t_2) complex points and 252 scans per FID. Spectra were processed with the NMRPipe/NMRDraw software and analyzed with the Sparky program.[91,92]

al strands are held together by double-helical regions (such as the hammerhead ribozyme shown in Figure 9A, below). In other RNAs it is not possible to form a stable functional molecule by combining multiple strands. To overcome this problem, Puglisi and co-workers have described a method for the ligation of differentially labeled strands utilizing T4 RNA ligase and have applied this to an NMR study of the 310-nucleotide internal ribosome entry site (IRES) RNA.[19] The T4 RNA ligase has specific nucleotide and loop-forming requirements for efficient ligation,[20] but if these criteria are met, it can give high yields for ligation. Figure 2 shows a schematic representation of the procedure in which a 50% yield of purified ligated IRES RNA was obtained. NMR studies showed that the secondary structure of the isolated domain II is the same as domain II in the full IRES RNA. Segmental-labeling approaches, with or without ligation, will be essential for studies of larger RNAs.

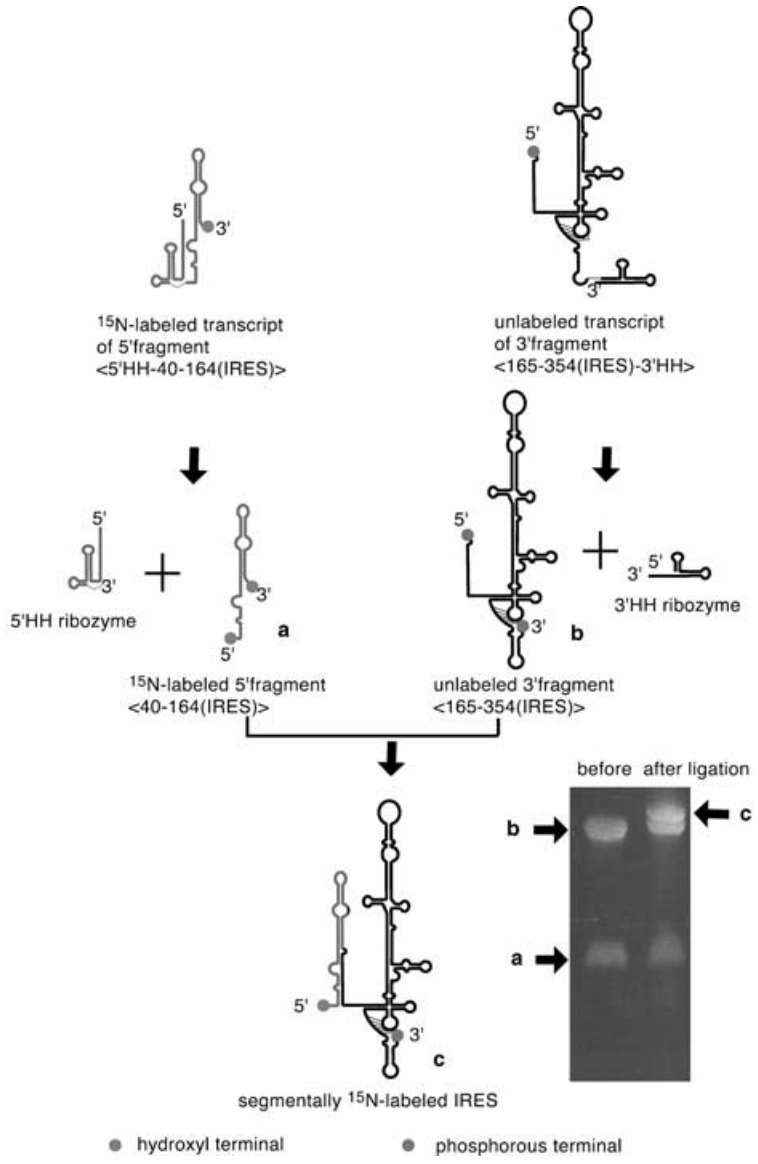

Figure 2. Schematic of the procedure for producing segmentally ^{15}N-labeled IRES RNA. Hammerhead ribozymes and in vitro transcription conditions were used to ensure that the proper 5′ and 3′ ends were produced for ligation by T4 ligase. Domain II is ^{15}N-labeled whereas the rest of the IRES RNA is unlabeled. Reproduced from ref. [19] with permission. Copyright (2002) American Chemical Society.

2.2. Improved methods for purification of RNA

After production of the RNA by in vitro transcription, the target RNA must be purified from the reactants, template, and abortive transcripts. Traditionally, denaturing (8 M urea) PAGE is used to purify RNA. This method has the advantage of being able to separate large quantities of RNA with single-nucleotide resolution. Two different HPLC strategies have been used to purify RNA: ion-pairing reversed-phase HPLC and denaturing anion-exchange HPLC.[21] For ion-pairing reversed-phase HPLC, a hydrophobic positively charged counter ion is used, and the RNA is eluted by increasing the concentration of this counter ion. For anion-exchange HPLC, heating of the column denatures the RNA, and increasing salt concentration elutes the RNA. In our experience these HPLC methods work well for separating smaller RNAs but are not able to resolve large RNAs (>30 nucleotides) as well as PAGE. All three of these techniques require that the purified RNA is desalted, dialyzed into appropriate buffer, and refolded into its active conformation.

Lukavsky and Puglisi have recently employed size-exclusion chromatography to purify large RNAs produced by in vitro transcription with T7 RNA polymerase.[22] Transcription from a linearized plasmid template often produces relatively pure transcripts for larger RNAs, especially when the transcript is processed to eliminate 3′ heterogeneity.[6] This method was used to produce a large IRES RNA (310 nucleotides). The restriction endonuclease and T7 RNA polymerase were removed from the transcription reaction by phenol/chloroform extraction. The target RNA was then purified away from the linearized template by size-exclusion chromatography. This method produced high-purity IRES RNA in NMR spectroscopy quantities.

A general, very efficient, affinity-tag-based purification procedure has recently been reported by Kieft and Batey.[23] The target RNA (RNA X in Figure 3) is cloned into a transcription vector containing both a mutant hepatitis delta virus ribozyme and an affinity-tag RNA on the 3′ side of the target RNA. The mutant hepatitis delta virus ribozyme requires high levels of imidazole for activity and therefore little or no cleavage occurs during the transcription reaction. The affinity tag consists of two stem loops from the *Thermotoga maritima* signal-recognition particle (SRP) RNA that bind with very high affinity to the *T. maritima* SRP protein Ffh. Figure 3 shows the general scheme for RNA purification. After in vitro transcription, the entire reaction is passed over an affinity column to which the

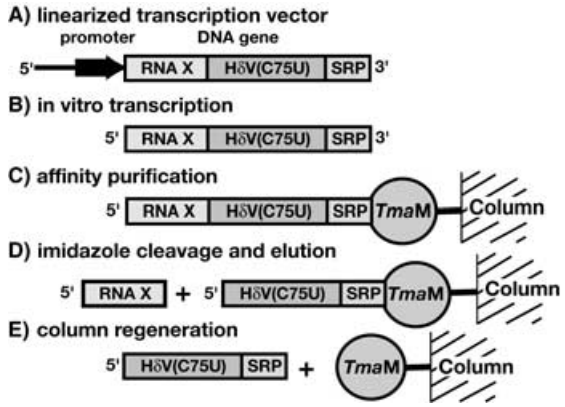

Figure 3. Schematic of the native purification procedure for in vitro transcribed RNA by using an RNA affinity tag. The RNA is put on an affinity column that has the *T. maritima* Ffh protein immobilized (*Tma*M) on it. The RNA of interest (RNA X) is removed from the SRP RNA affinity tag by cleavage of the hepatitis delta virus (HδV) mutant C75U with imidazole. The column can be regenerated by addition of EDTA because the RNA affinity tag does not bind to the Ffh protein in the absence of Mg^{2+}. Reproduced from ref. [23] with permission. Copyright (2004) Cold Spring Harbor Laboratory Press.

T. maritima Ffh protein has been immobilized. Full-length transcripts bind to the column and incomplete transcripts and unincorporated nucleotides are eluted. The target RNA is then cleaved by the addition of imidazole and eluted from the column. Washing with high concentrations of ethylenediaminetetraacetate (EDTA) can regenerate the column because the affinity tag SRP RNA does not bind in the absence of Mg^{2+}. This procedure enormously facilities the purification of homogenous length RNA and is likely to become the standard method for large-scale production of RNAs. Another advantage of this method is that it avoids denaturing the RNA, which may be important for obtaining fully active larger RNAs.[23]

3. Direct Detection of Hydrogen-Bonding Interactions

The HNN-COSY experiment represents a powerful method for directly observing hydrogen-bonding interactions in ^{15}N-labeled nucleic acids. For standard Watson–Crick base pairs, this experiment correlates the donor and acceptor nitrogen atoms for hydrogen bonds involving the T/U or G imino protons.[24,25] Figure 4 schematically shows the magnetization transfer pathway for this experiment in A–U and G–C base pairs. The critical aspect of this experiment is that magnetization is transferred across the hydrogen bond through the two-bond scalar coupling ($^2J_{NN'}$). The HNN-COSY experiment very efficiently transfers magnetization and therefore can be applied to larger RNAs, as illustrated by the spectrum of ^{15}N-labeled native $tRNA^{Val}$ shown in Figure 4.

The sizes of the $^2J_{NN'}$ coupling constants have been measured for canonical and noncanonical base–base interactions in a variety of DNA and RNA systems, and both empirical and theoretical studies have correlated hydrogen-bond strengths and lengths with the measured $^2J_{NN'}$ coupling constants.[24–33] As a larger database of these $^2J_{NN'}$ coupling constants becomes available, it may be possible to incorporate this coupling constant data directly into RNA structure refinements.

It is also possible to directly observe hydrogen-bonding interactions for an imino proton donor and carboxyl oxygen acceptor in HN(N)-TOCSY and long-range H(N)CO experiments which transfer magnetization through $^4J_{NN}$ and $^3J_{NC'}$ couplings, respectively.[27,34] These are more challenging experiments due to the additional magnetization transfers and the smaller size of these couplings, and thus, the application of these methods to larger RNAs may be more limited.

The HNN-COSY experiment and its variants have been used to unambiguously determine specific base-pair formation in a variety of nucleic acids.[26,27,35,36] This experiment has also been used to distinguish between possible secondary structures in RNAs. Since there is a large chemical shift dispersion of the nitrogen signals, the types of nitrogen atoms involved in the hydrogen bond (N1, N3, N7, or N9) can often be determined. Butcher and co-workers utilized this strategy to define the secondary structure of the U2–U6 small nuclear RNA from the *Saccharomyces cerevisiae* spliceosome complex.[37] The 73-nucleotide construct contained the region in the U2–U6 RNA complex closest to the pre-mRNA binding site. The ^{1}H,^{1}H-NOESY and HNN-COSY experiments identified a G–U wobble and two U–U base pairs, thus indicating that this RNA forms a four-way junction.

The HNN-COSY experiment was also applied to adenine and guanine riboswitches by Schwalbe and co-workers.[38] These purine-sensing RNAs specifically bind adenine or guanine as part of the regulation mechanism in the metabolic pathway of these bases. The HNN-COSY experiment was used to identify hydrogen-bond donors and acceptors involved in the specific recognition of the ligand by the individual riboswitches. For example, the HNN-COSY spectrum of the complex between a ^{15}N-labeled adenine ligand and a ^{15}N-uridine-labeled adenine riboswitch revealed a Watson–Crick base pair between the adenine ligand and a uridine residue in the riboswitch (Figure 5). An analogous Watson–Crick interaction was observed between the guanine ligand and a cytidine residue in the guanine riboswitch. Hydrogen-bonding interactions were also detected between the N3/N9 face of the adenine ligand and the N3 of a uridine residue in the riboswitch, as illustrated in Figure 5. By combining data for the various base-pairing interactions, the specific mechanism that each riboswitch uses to discriminate between purine bases was determined.[38]

The two studies presented above did not rely upon complete resonance assignments. Instead, ^{1}H,^{1}H correlations from NOESY experiments and hydrogen-bonding interactions from HNN-COSY experiments were used to determine the secondary structure or the mechanism for ligand binding. These examples demonstrate how NMR spectroscopy can be used to unambiguously identify standard secondary structure, noncanonical base pairing, and novel ligand–RNA interactions in RNAs.

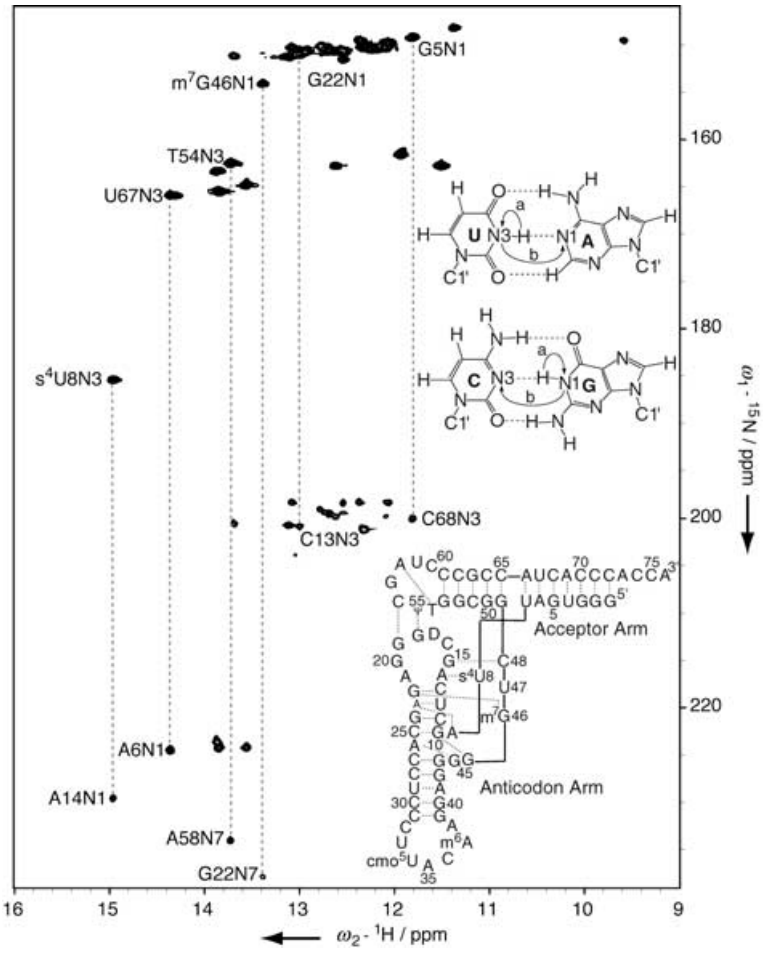

Figure 4. Imino region of the 2D HNN-COSY spectrum of uniformly ^{15}N-labeled native tRNA^{Val} with some representative $J_{NN'}$ correlations highlighted. The upper inset shows the magnetization transfer steps for the 2D HNN-COSY. Magnetization is transferred from the imino proton to the imino nitrogen (arrow labeled a). The magnetization is then transferred across the hydrogen bond during a mixing time (arrow labeled b). After frequency labeling in t_1, the magnetization is transferred back to the imino proton through the reverse process. The lower inset shows the secondary structure of the native *E. coli* tRNA^{Val} used in this study. Peaks below 190 ppm in the ^{15}N dimension are of the opposite sign. ^{15}N-labeled native tRNA^{Val} was overexpressed and purified as described in the legend of Figure 1. This HNN-COSY experiment was preformed on a 600 MHz Varian INOVA spectrometer equipped with a pulsed-field gradient HCN probe at 25 °C. 512 × 1024 complex points and sweep widths of 5900 and 20 000 Hz were collected in t_1 and t_2. The ^{15}N carrier was set at 186.7 ppm. A mixing time of 15 ms was used for the NN-COSY transfer step. A total of 128 scans were taken per FID. Spectra were processed with the NMRPipe/NMRDraw software and analyzed with the Sparky program.[91,92]

4. Applications of Residual Dipolar Couplings for Probing the Structure and Dynamics of RNA

Proton–proton distance constraints derived from ^{1}H,^{1}H nuclear Overhauser effects and torsion-angle constraints derived from three-bond scalar coupling constants provide tremendous amounts of short-range data for determining the local structure of macromolecules in solution. However, these data do not provide long-range structural information, thereby limiting the extent to which the global structure of a molecule can be determined. The lack of long-range structural data is especially critical in nucleic acids, where the local double-helical structure can be precisely determined but it is usually not possible to determine the extent of a helical bend or the relative orientations of helical regions.[39]

Thus the ability to obtain high-resolution multidimensional NMR spectra in partially ordered systems, facilitating measurement of residual dipolar couplings (RDCs), is revolutionizing global-structure determinations of nucleic acids.[40–42] In normal isotropic solutions, dipolar couplings average to zero; however, partial ordering leads to "residual" dipolar couplings. If the distance between two NMR-active nuclei is known (for example, in bonded ^{1}H–^{15}N or ^{1}H–^{13}C groups), the relative orientation of these internuclear vectors can be determined. RDCs provide a large number of long-range structural constraints that complement the standard NOE and *J* coupling constant data, therefore allowing for more accurate determination of global structures of large RNAs.[42]

4.1. Improved pulse sequences for measurement of RDCs in RNA

A wealth of information for the local and global structure of proteins is being obtained from backbone ^{1}H–^{15}N one-bond RDCs.[42] However, ^{15}N labeling in RNA only yields a limited number of ^{1}H–^{15}N RDCs, because many of the G and U imino proton resonances are not observed due to rapid exchange with water. Only the subset of imino protons that form stable intra- or intermolecular hydrogen-bonding interactions can be used to measure RDCs. Therefore, ^{13}C labeling (or ^{13}C at natural abundance) is needed for measuring one-bond ^{1}H–^{13}C RDCs. The best resolved and most easily measured one-bond ^{1}H–^{13}C RDCs are those of C2–H2 in adenine, C8–H8 in purines, C5–H5 and C6–H6 in pyrimidines, and the ribose C1′–H1′. Spectral overlap in standard 2D ^{1}H,^{13}C-HSQC experiments limits the number of one-bond residual dipolar couplings that can be obtained for other groups in the ribose rings of RNAs.

Hydrogen-bonding interactions between aromatic bases are the major determinate for secondary structure formation in nucleic acids. Thus, the relative orientations of the bases, including detailed helical parameters, are commonly used to describe nucleic acid structures.[43] Since the bases have a fixed geometry, only three linearly independent RDCs are needed to predict all other RDCs in the planar base ring.[44,45] However, measurement of additional base RDCs improves the accuracy of the RNA structure determinations.

Various methodologies have been recently developed for generating additional RDC data for the bases in RNAs. Three suites of experiments have been described for measuring one- and two-bond RDCs in the base, as well as between the N1/N9 and C1′ atoms in RNAs.[44–46] Sklenár and co-workers utilize spin-state-selective excitation experiments to measure 8–10 RDCs in the purine rings and 10–15 RDCs in the pyrimidine

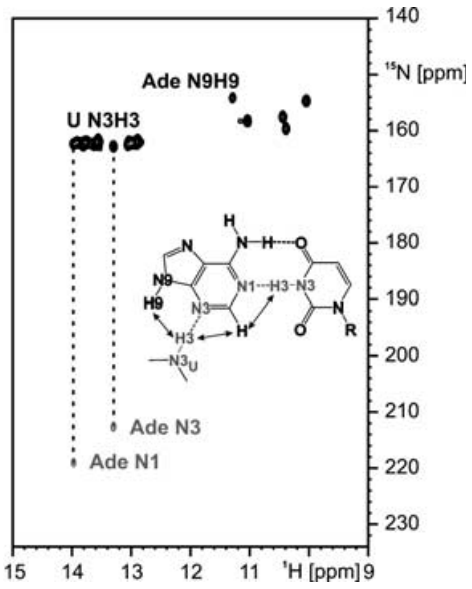

Figure 5. Imino region of the 2D HNN-COSY spectrum of the ^{13}C,^{15}N-uridine-labeled adenine-responsive riboswitch in complex with ^{13}C,^{15}N-labeled adenine. Correlations between two uridine imino groups on the RNA and the N1 and N3 of the adenine are shown as dashed lines, unambiguously identifying hydrogen bonding between these groups. The inset shows N–H···N hydrogen-bonding interactions deduced from the HNN-COSY spectrum. Arrows indicate correlations seen in ^{1}H–^{1}H NOESY spectra. Reproduced from ref. [38] with permission. Copyright (2005) National Academy of Sciences.

rings.[44] Bushweller and co-workers described a suite of six multiple-quantum HCN-based experiments to measure four purine and six pyrimidine one- and two-bond RDCs around the C6/8 and C1′ atoms.[46] Bax and co-workers described 3D-TROSY-based pulse sequences for the measurement of three or four RDCs in purines and seven RDCs in pyrimidines.[45] Scheme 1 shows which RDCs can be measured for each of these three approaches. New experiments are also being developed for the assignment of quaternary carbon signals in the bases,[47,48] thereby providing additional avenues for measuring base RDCs.

Given the numerous torsion angles in the sugar–phosphate backbone of nucleic acids, it is challenging to adequately define the backbone structure of nucleic acids from NMR data. By using standard NOE and torsion angle data, the critical structural information used to determine the conformation of the sugar-phosphate backbone is most likely to be derived from distance constraints between the bases, instead of constraints for the sugar or phosphate groups. Thus, additional structural data on the sugar–phosphate backbone will lead to higher resolution RNA structures.

Bax and co-workers have developed a suite of 2D and 3D experiments where up to five one-, two-, and three-bond RDCs can be measured for the ribose sugar (as well as the sum of various RDCs).[49,50] These methods focus on the simultaneous measurement of RDCs involving the ribose C5′–H5′/H5′′ group, as well as the H1′–C1′–C2′–H2′ group, as illustrated in Scheme 2. In some of these experiments, several RDCs are measured multiple times to provide higher precision and accuracy for the RDCs. Valluru-palli and Moore, as well as Bax and co-workers, have developed 3D HcCH-COSY and 3D relay HcCH-COSY experiments that reduce spectral overlap, thereby yielding additional RDCs for the C2′–H2′ and C3′–H3′groups.[51,52] A 3D experiment has also been developed for improved measurements of three-bond C2′–P and C4′–P RDCs.[53] Some of these techniques have only recently been developed, and thus they have yet to be generally applied. It will be interesting to see how these additional RDC constraints for the sugar and phosphate moieties improve the quality of NMR structure determinations of RNA.

The procedures described above have focused on the measurement of RDCs for nuclei separated by one, two, and three bonds. Long-range ^{1}H–^{1}H residual dipolar couplings, containing distance and orientational information, can also be measured. The $1/r^3$ distance dependence has been used in our laboratory to measure long distances ($\approx$7 Å) between isolated H2 protons in adenines in a DNA double helix,[54] but the large number of short-range ^{1}H–^{1}H RDCs hinders practical measurement of most long-range ^{1}H–^{1}H RDCs. Bax and co-workers have recently demonstrated a procedure for removing homonuclear couplings outside a selected bandwidth.[55] This selection procedure was applied to H1′ and H5 resonances, and several RDCs between protons separated by over 9.0 Å were observed. These long-range distance and orientational constraints will provide additional data for calculating structures by using only RDC data.

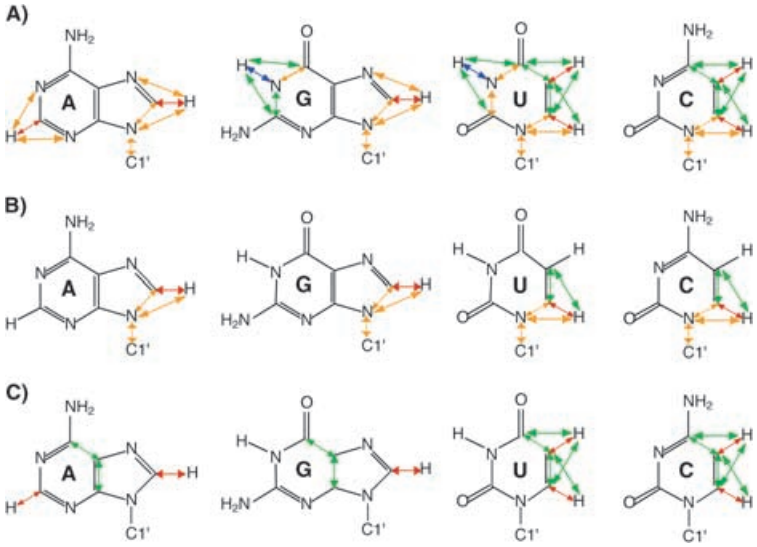

Scheme 1. One- and two-bond RDCs that can be measured in bases by various NMR experiments. The $^{1}D_{NH}$ value here is set to 25 Hz, and the color of an arrow represents the relative magnitude of the RDC (red = 50 Hz, blue = 25 Hz, green = 6–8 Hz, orange = 2–3 Hz). The set of RDCs that can be measured from A) three HCN, HNC, and HCC experiments developed by Sklenár and co-workers,[44] B) six 3D multiple quantum HCN-based experiments developed by Bushweller and co-workers,[46] and C) two 3D TROSY-based experiments developed by Bax and co-workers.[45]

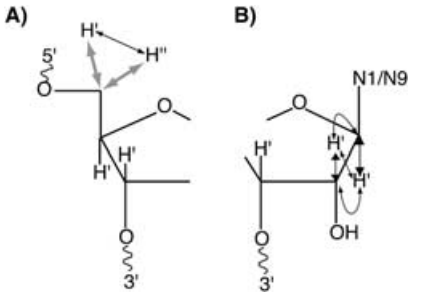

Scheme 2. One-, two-, and three- bond RDCs that can be measured in the ribose ring by 2D and 3D $^{1}H,^{13}C$ correlation experiments. A narrow black arrow indicates that a single RDC is measured and a thick grey arrow indicates the sum of two RDCs. A) The $^{1}D_{C5'H5'}$, $^{1}D_{C5'H5''}$, and $^{2}D_{H5'H5''}$ values are measured in a 2D spin-state-selective HSQC.[49] B) A set of five RDCs for the H1′–C1′–C2′–H2′ are measured from a single 3D HCC experiment.[50]

4.2. Determining the global structure of larger RNAs from RDC data

Our group has used RDCs to determine the helical stem orientations for several different tRNAs as well as the three stems in the minimal construct of the hammerhead ribozyme.[14,56,57] Analysis of the $^{1}H–^{15}N$ RDCs showed that the helical domains in ^{15}N-labeled native tRNA^{Val} orient as a single rigid species; this means that these data can be used to determine the relative orientation of the two helical arms in the tRNA.[56] These studies showed that, by assuming an A-form geometry for the double-helical stems, it is possible to determine the global fold of the tRNA from a relatively small number of RDCs (27 in total). Figure 6 shows a comparison of a model for tRNA^{Val} derived from the X-ray crystal structure of tRNA^{Phe} and the model for tRNA^{Val} determined from the RDC data. The calculated angle between the two arms was 99°, whereas angles of 76–96° have been observed in the 4 crystal structures of free tRNAs. More recent studies that compared the global structure and dynamics of native and unmodified tRNA^{Val}[14] used simulations to show that structural noise,[58] as opposed to uncertainties in RDC values or in estimates of alignment-tensor magnitudes, was the primary source of imprecision in determining the global structure of helical domains in RNAs.

The global structure of the minimal hammerhead ribozyme has been determined from a set of $^{1}H–^{15}N$ and $^{1}H–^{13}C$ RDCs, complemented with additional NOE restraints.[57] The hammerhead ribozyme consists of three helical regions surrounding a conserved catalytic core. The determination of the global orientation of three domains represents a major challenge if the RDCs are all obtained from a single alignment tensor. RDC data have a $4^{(n-1)}$-fold degeneracy for determining the global orientation of any number of n domains, which leads to 16 possible solutions for this 3-domain hammerhead system.[57,59] Although most of the 16 solutions were ruled out by the covalent structure, other data, such as NOE restraints, were required to select the correct conformation. The results show that the hammerhead ribozyme has a rather extended structure in solution in the absence of Mg^{2+} (Figure 7). This global structure is very different from the more compact Y-shaped X-ray crystal structure determined in the presence of Mg^{2+}.

The NMR spectroscopy solution structure of the IRES domain II was determined by Puglisi and co-workers, with RDC data providing the global-structure information.[60] The IRES domain II contains two subdomains (IIa and IIb), and local structural restraints were obtained from NMR studies on each of the smaller subdomains. This local structural information was combined with the RDCs for the entire molecule to yield the final structure of the entire domain. The inclusion of this RDC data dramatically improved the structure determination of the entire domain II and reduced the root mean square deviation (rmsd) from 7.48 to 2.18 Å, as illustrated in Figure 8. Inclusion of these global restraints made it possible to determine 2 helical bend angles, the first of approximately $85 \pm 10°$ within subdomain IIa between the upper and lower portions of domain II and the second of approximately $47 \pm 13°$ within subdomain IIb between a loop E motif and an

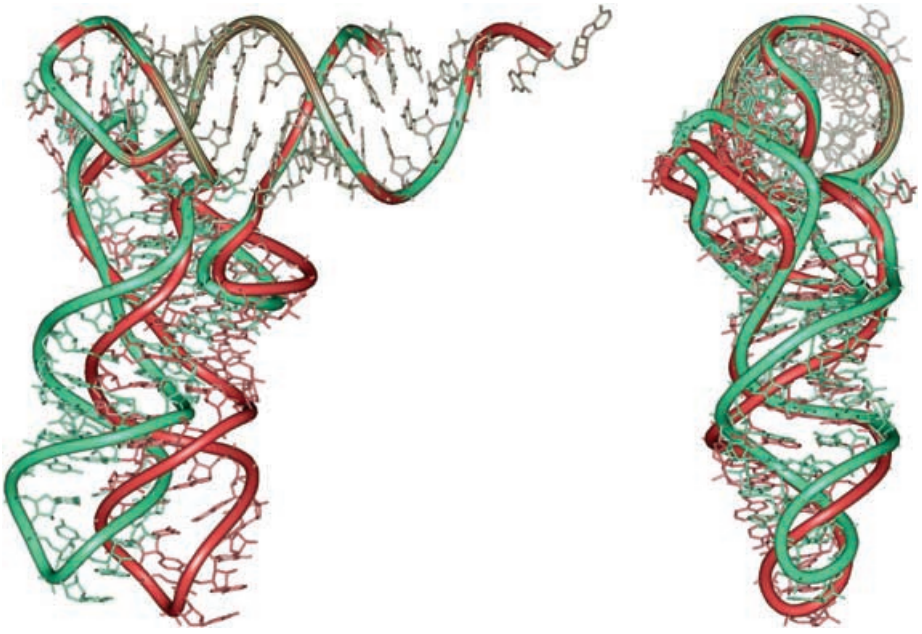

Figure 6. Comparison of the X-ray crystal structure model for native *E. coli* tRNA^{Val} (in red) with the global structure determined from $^{1}H–^{15}N$ imino RDC data on native *E. coli* tRNA^{Val} (in green). The structure from the RDC data assumed A-form geometry for the acceptor and anticodon helical arms. The X-ray crystal structure model for the *E. coli* tRNA^{Val} was derived from the X-ray crystal structure for yeast tRNA^{Phe}. The acceptor arms in the two structures are superimposed. The structures on the right are rotated by 90°. Reproduced from ref. [56] with permission. Copyright (2000) American Chemical Society.

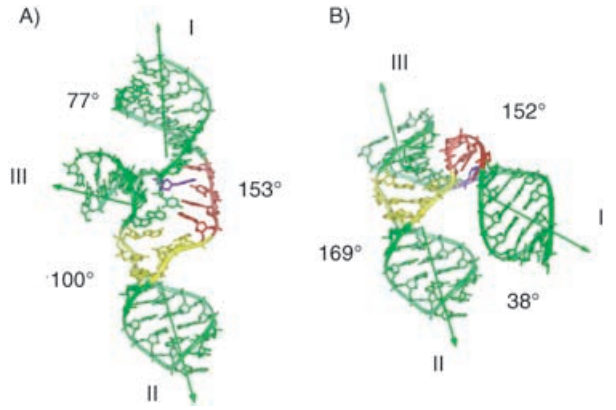

Figure 7. Global conformations of the minimal hammerhead ribozyme A) determined in solution from $^{1}H–^{15}N$ and $^{1}H–^{13}C$ RDC data in no Mg^{2+} conditions and B) the X-ray crystal structure in the presence of Mg^{2+}. The interstem angles are shown and the conserved core residues are shown in yellow, red, and purple. Reproduced from ref. [57] with permission. Copyright (2002) American Chemical Society.

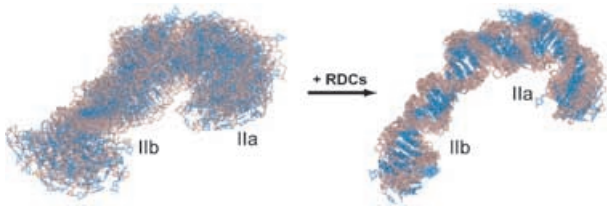

Figure 8. Solution structure of IRES domain II. The heavy-atom superimposition of the final family of 20 structures on the left was calculated with only NOE and *J* coupling constant restraints. The superimposition of 12 structures on the right illustrates the improvement in global structure by also including RDC restraints. The addition of these RDC restraints lowered the overall rmsd from 7.48 to 2.18 Å. Reproduced from ref. [60] with permission. Copyright (2003) Nature Publishing Group.

asymmetrical bulge. Thus, RDC data can be used to determine global structures and orientations and have been successfully applied to RNAs larger than 25 kD.

4.3. Methods for aligning RNA for measurement of RDCs

One method for creating anisotropic solutions for RDCs simply utilizes the magnetic susceptibility of a molecule to align in a magnetic field.[61] This alignment scales with the square of the magnetic field, and the RDCs are extracted from analysis of coupling data at multiple fields. Magnetic-field alignment of macromolecules is becoming more feasible with the availability of ultrahigh field (800 and 900 MHz) NMR systems and may be especially valuable for measuring RDCs in nucleic acids, due to the large magnetic susceptibility of DNA and RNA double helices.[62,63] Although magnetic alignment is the least perturbing method for measuring RDCs, it is limited because the degree of alignment cannot be modulated at a given magnetic field. Thus, a large number of different alignment media have been developed for proteins and nucleic acids, with Pf1 filamentous phage, bicelles, and polyacrylamide gels being the most widely used in RDC studies.[42]

Measurement of multiple alignment tensors enormously simplifies the global-structure determination of macromolecules in solution. This is because analysis of RDC data from two or more independent alignment tensors eliminates the natural fourfold degeneracy for orienting two domains from RDCs.[64] It is not easy to obtain several independent alignment tensors for nucleic acids, because most of the current alignment media yield essentially equivalent alignment tensors for a given DNA or RNA (unpublished results). The two most promising methods for obtaining independent alignment tensors in studies of RNA are magnetic-field alignment and paramagnetic alignment. One of the earliest measurements of RDCs in nucleic acids utilized a paramagnetic metal to align a G-quartet system.[65] The G-quartet has natural strong metal-binding sites where a variety of metals can bind without significantly changing the structure of the G-quartet. However, in many RNA systems, paramagnetic metals lead to alternative, often inactive or incorrectly folded, structures. Thus, a more general approach will be to develop paramagnetic tags[66] that can be connected to an RNA, thereby leading to a very different alignment tensor for the molecule. As ultrahigh magnetic fields and easily incorporated nonperturbing paramagnetic tags become more available, these techniques will become valuable tools for the alignment of RNAs.

4.4. Studies of RNA dynamics from RDC data

RDCs can also be used to obtain information on dynamics in macromolecules.[67] Bax and co-workers analyzed a large number of RDCs in the Dickerson dodecamer and showed that some sugar rings in the DNA duplex were undergoing rapid conformational exchange between 2′-*endo* and 3′-*endo* sugar puckers.[68] In another example of the analysis of conformational dynamics from RDC data, Patel and co-workers extracted the amplitude and direction for the motions of the two helical domains in the HIV-1 TAR RNA.[69,70] The TAR RNA consists of two helical domains separated by an asymmetric three-nucleotide bulge. The RDCs were analyzed to determine whether the two domains orient with the same alignment-tensor magnitudes. For rigid domains, the alignment-tensor magnitudes (or equivalently the generalized degree of order (ϑ) and the asymmetry parameter (η)) for the individual domains should be identical.[71] In studies on the tRNA, hammerhead, and IRES systems (discussed in Section 4.2), similar alignment tensors were observed for individual domains in each of these RNAs; this is consistent with the RNA orienting as a single rigid species. However for the TAR RNA in the absence of Mg^{2+}, large differences were observed in ϑ values between the two stems; this suggests that these helical domains experience different degrees of alignment and therefore are not orienting as a single rigid species.[69] The amplitudes of the motion can then be estimated from analysis of the RDC data, but this is challenging since the results depend upon the particular motional model employed. A cone model of motion was employed for the TAR RNA and gave an amplitude of motion of $\approx 46°$ between the helical domains. Additional RDC studies on the molecule in the presence of 4.5 mM Mg^{2+} showed no evidence for interdomain

motion in TAR,[70] thereby demonstrating that Mg^{2+} affects not only the structure but also the dynamics of RNA in solution.

5. NMR Relaxation Studies of Microsecond to Millisecond Dynamics in RNAs

A better understanding of the biological function of RNA requires information on both the structure and dynamics of the molecule. The conformational dynamics that are important for biological activity occur over a wide range of timescales. Fast librational motions on the ps to ns timescale allow molecules to sample multiple conformations with small energetic barriers. NMR techniques have been used to study slower μs to ms timescale motions such as stem reorientations,[71] base-pair opening,[72] sugar-pucker conformational averaging,[73] and base flipping.[74] Heteronuclear spin relaxation measurements represent a powerful approach for probing conformational changes occurring on these slower timescales. These methods are commonly used in protein systems but have only more recently been applied to RNAs.[75–77]

Motions on the μs timescale can be studied by analysis of the power dependence of transverse rotating-frame relaxation rates ($R_{1\rho}$). The $R_{1\rho}$ experiment employs a variable-length spin-lock field to continuously refocus the transverse magnetization.[78] The dependence of the $R_{1\rho}$ value on the strength of the spin-lock field gives information on the chemical exchange lifetime (τ_{ex}) between two states according to Equation (1), where $R_{1\rho}$ is the measured relaxation time, p_a and p_b are the fractional populations of the two states, $\Delta\omega$, is the chemical shift difference between the two states, ω_1 (where $\omega_1 = \gamma B_1 = 2\pi\nu_1$) is the spin-lock power (in rad s^{-1}), and $R_{1\rho}^{\infty}$ is the relaxation time at infinite spin-lock power.[79,80] The rate constant for the exchange process, $k_{ex} = \tau_{ex}^{-1}$, is the sum of the forward and reverse microscopic rate constants for two-site exchange.

$$R_{1\rho} = R_{1\rho}^{\infty} + p_a p_b (\Delta\omega)^2 \frac{\tau_{ex}}{1+\omega_1^2\tau_{ex}^2} \quad (1)$$

Here we present the analysis of the power dependence of $R_{1\rho}$ to probe the dynamics in the small catalytic RNA, the minimal hammerhead ribozyme.[81,82] The sequence and secondary structure of the hammerhead ribozyme–substrate complex are shown in Figure 9 A. We employed a ^{13}C,^{15}N-adenosine-labeled ribozyme strand complexed with an unlabeled noncleavable substrate strand (in a 1:1 ratio). For RNAs, the purine C8 and C2 spins are excellent candidates for power dependence of $R_{1\rho}$ measurements because they are not complicated by the ^{13}C–^{13}C cross-correlated relaxation observed for the sugar and the pyrimidine C5/C6 spin systems.[83,84] A series of $R_{1\rho}$ experiments were performed on the hammerhead complex in the absence of Mg^{2+} by using 12 spin-lock times ranging from 4–50 ms and 6 spin-lock powers (ν_1) ranging from 1.00–6.70 kHz.

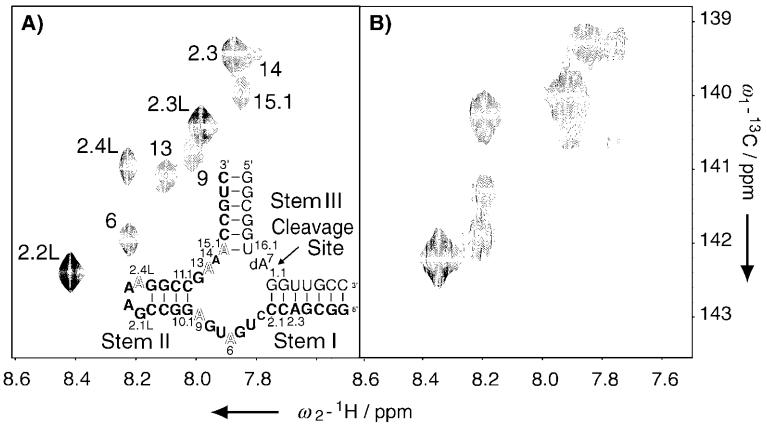

Figure 9. The aromatic region of 2D ^1H,^{13}C $R_{1\rho}$ spectra of the ^{13}C,^{15}N-adenosine minimal hammerhead ribozyme A) in the absence of Mg^{2+} and B) with 1.0 mM Mg^{2+}. The inset shows the sequence and secondary structure of the minimal hammerhead ribozyme where the bold typeface is the ^{13}C,^{15}N-adenosine labeled enzyme strand and the regular typeface is the unlabeled substrate strand with a noncleavable deoxyribose at the cleavage site. Adenosine residues with C8 resonances that have significant power dependence for $R_{1\rho}$ in no Mg^{2+} conditions are outlined in the secondary structure. Both 2D spectra employed a spin-lock time of 4 ms with spin-lock powers of 2255 and 1791 Hz, with and without Mg^{2+}, respectively. Assignments of adenosine H8–C8 resonances in no Mg^{2+} conditions are shown.[57] As seen in (B), some adenosine H8–C8 resonances exhibit line broadening upon addition of Mg^{2+}. Samples consisted of 0.8 mM complex, 100 mM NaCl, 25 mM $^2H_4$-succinate, and 0.1 mM EDTA (pH 5.5) in 100% ^2H_2O. All $R_{1\rho}$ experiments were performed on a 500 MHz Varian INOVA spectrometer at 25 °C and employed a spin-lock sequence during the relaxation delay[78] with a modification to include a 180° ^{15}N-decoupling pulse during the t_1 period. Spectra were acquired with 80 complex points in the indirect dimension and 32 scans per FID and were processed with the NMRPipe/NMRDraw software and viewed with the Sparky program.[91,92]

The $R_{1\rho}$ relaxation rates were determined by fitting the extracted peak volumes to a single-exponential decay function. The effective spin-lock field, ω_{eff}, for individual resonances was corrected for off-resonance effects with Equation (2), where Ω is the resonance offset (in rad s^{-1}) from the applied B_1 field.

$$\omega_{eff} = (\omega_1^2+\Omega^2)^{1/2} \quad (2)$$

The observed $R_{1\rho}$ rates, $R_{1\rho}^{obs}$, also contain contributions from both transverse and longitudinal relaxation and were corrected for the rotating-frame axis tilted off-resonance from horizontal according to Equation (3), where $\theta = \tan^{-1}(\omega_1/\Omega)$ is the angle of the axis from vertical.[85] The variation for the tilt angles (θ = 76–88° and 86–89° at 1.00 and 3.60 kHz, respectively) results from resonance offsets ranging from 44–245 Hz (maximum for A2.3 C8 in the hammerhead system; Figure 9).

$$R_{1\rho}^{obs} = R_1\cos^2\theta + R_{1\rho}\sin^2\theta \quad (3)$$

The $R_{1\rho}^{\infty}$ value in Equation (1) was estimated from Equation (4), where $\langle R_{1\rho}/R_1\rangle$ is the average ratio for residues that show no evidence of chemical exchange (A2.3 and A2.3L in the hammerhead system; Figure 9).

$$R_{1\rho}^{\infty} = \left\langle \frac{R_{1\rho}}{R_1} \right\rangle R_1 \quad (4)$$

The use of this $\langle R_{1\rho}/R_1\rangle$ ratio to calculate $R_{1\rho}$ assumes an isotropic correlation time.The corrected $R_{1\rho}$ rates as a function of

ν_{eff} (Figure 10) are fitted to Equation (1) by using a two-parameter nonlinear Levenberg–Marquardt least-squares minimization with weighted error propagation to give $p_a p_b(\Delta\omega)^2$ and τ_{ex}.

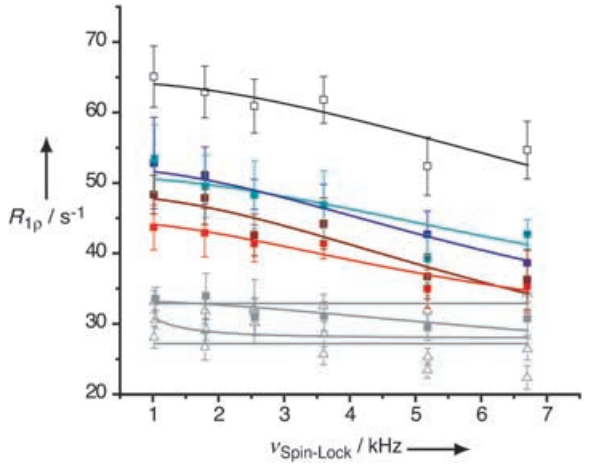

Figure 10. Power dependence of the corrected $R_{1\rho}$ for the C8 resonances in the ^{13}C,^{15}N-adenosine-labeled minimal hammerhead ribozyme. Residues in the core are indicated by filled symbols whereas residues in helices and the GAAA tetraloop are indicated by open symbols. The C8 resonances for core residues A6, A9, A13, A15.1, and A2.4L in the tetraloop (red, blue, brown, cyan, and black squares, respectively) show significant power dependence. C8 resonances that show little or no power dependence are shown in gray. The curves correspond to the two-parameter fitting of $R_{1\rho}$ rates measured at each ν_{eff} value to Equation (1), with parameter values summarized in Table 1. The inset of Figure 9A maps the residues with power dependence (outlined) onto the secondary structure of the hammerhead ribozyme.

Four of the five adenosines in the core (A6, A9, A13, and A15.1) show exchange lifetimes for their C8 positions of 19–27 μs; this demonstrates that the core is highly dynamic (Table 1). It is not possible to tell if these effects arise from concerted motions within the core or if these residues are experiencing independent dynamics on the μs timescale. Residue A2.4L in the GAAA tetraloop also shows a strong power dependence of $R_{1\rho}$, with this C8 experiencing chemical exchange with a lifetime $\approx$16 μs. These results demonstrate substantial dynamics in the conserved core of this minimal hammerhead ribozyme in the absence of Mg^{2+}.

Table 1. Chemical-exchange parameters for C8 positions of adenosine residues in the minimal hammerhead ribozyme.[a]

Base	$R_{1\rho}^{\infty}$ [s^{-1}]	Ω [Hz]	τ_{ex} [μs]	$p_a p_b(\Delta\omega)^2$ ($\times 10^5$)
A6	27	44	27 ± 8.5	6 ± 1.4
A9	24	77	23 ± 6.1	12 ± 2.4
A13	17	55	22 ± 4.6	14 ± 2.4
A15.1	26	178	19 ± 4.7	13 ± 2.2
A2.4L	25	44	16 ± 4.0	25 ± 2.2

[a] Data were extracted from a two-parameter fit of the power dependence of $R_{1\rho}$ to Equation (1) (see text). $R_{1\rho}$ data were acquired with spin-lock times of 4, 6, 8, 10, 14, 18, 22, 26, 30, 36, 42, and 50 ms and with spin-lock powers of 1010, 1790, 2540, 3600, 5180, and 6700 Hz.

RDC data were used to show that the minimal hammerhead ribozyme forms an extended conformation in solution in the absence of Mg^{2+} (see Section 4.2).[82] To achieve an active conformation, the minimal ribozyme must undergo a Mg^{2+}-dependent conformational rearrangement that brings stems I and II into proximity while also reorganizing the core residues for in-line attack of the 2′OH with the scissile phosphate group.[81,86] The exchange lifetimes reported here for the adenine residues in the core provide information on the dynamics of the hammerhead ribozyme in its extended conformation. Analogous $R_{1\rho}$ experiments on the hammerhead ribozyme in the presence of 1.0 mM Mg^{2+} show no power dependence of $R_{1\rho}$ for any adenosine residues (data not shown). However the 2D ^{1}H,^{13}C $R_{1\rho}$ spectrum of the minimal hammerhead complex with 1.0 mM Mg^{2+} does show evidence for chemical-exchange line broadening for some adenosine residues (Figure 9B). Thus, ^{13}C T_2-CPMG experiments were performed on this hammerhead complex to probe for longer (ms) timescale motions. Unfortunately the multiple ^{13}C–^{13}C couplings to the C8 from other carbon atoms in the adenine ring interfere with the analysis of the T_2-CPMG data. The C8 and C4/C5/C6 carbon atoms all resonate in a similar spectral region, thereby making it impossible to effectively decouple the C8 from the C4, C5, and/or C6 carbon atoms. Thus, the two- and/or three-bond ^{13}C–^{13}C J couplings dominated the apparent relaxation in the T_2-CPMG experiments. Therefore, we were unable to determine whether there are any slow (ms) exchange processes for the adenosine C8 spins in the hammerhead ribozyme with 1.0 mM Mg^{2+}.

As discussed in Section 2.1, we have developed a procedure for selective labeling of C8 in purines by growth on ^{13}C-formate, and samples prepared by this method will not have any ^{13}C–^{13}C couplings. This should make it possible to acquire ^{13}C T_2-CPMG data on the hammerhead ribozyme without the interference from ^{13}C couplings. Furthermore, recent biochemical studies on the hammerhead ribozyme show that if a naturally occurring loop–loop tertiary interaction involving stems I and II is added to the minimal construct, the ribozyme shows activity at low Mg^{2+} concentrations (100 μM) and also has 100-fold faster rates at higher Mg^{2+} concentrations.[87,88] It will be interesting to see how a tertiary interaction between two loops that are distant from the active site affects the structure and dynamics of the residues in the conserved core.

6. Summary

The high degree of spectral overlap in unlabeled oligonucleotides severely limits the application of solution NMR techniques for RNAs. The development of efficient methods for the production of isotopically labeled RNAs in the early 1990s dramatically changed the extent to which NMR spectroscopy could be used for studies on RNA.[9,10,89] The production of ^{13}C- and ^{15}N-labeled RNAs allowed a wide range of heteronuclear multidimensional NMR techniques to be applied to RNAs and made it possible to routinely determine the solution structures of small- to moderate-sized RNAs. Another revolutionary advance in structure determinations by NMR spectroscopy was the development of liquid-crystal methods for partially ordering bio-

molecules in solution, as reported by Tjandra and Bax in 1997.[40] The development of tunable orientation media permitted the application of powerful RDC methods to solution NMR studies of biomolecules. Novel applications of RDC data to biomolecules continue to be developed, with the vast majority of these studies being performed on protein systems. More recently, a growing number of NMR techniques have been developed for using RDC data to probe nucleic acid structure and dynamics. The long-range structural information provided by RDCs will probably have a much greater impact in studies of nucleic acids than in proteins, due to the extended secondary structure and limited number of NOE constraints in DNA and RNA oligomers. Thus, the ability to measure large numbers of RDCs should significantly improve structure determinations of RNA. Another important advance in NMR studies of RNAs has been experiments that directly observe hydrogen-bonding patterns in DNA and RNA. In general, Watson–Crick base pairs can be accurately determined by standard NOE techniques; however, the ability to directly identify hydrogen-bonding partners allows noncanonical base–base interactions to be unambiguously defined.

It is becoming increasingly clear that a detailed understanding of the molecular function of a biomolecule requires information on both the molecule's structure and dynamics. RNAs have long been known to adopt alternative conformations in solution;[90] however, methods for determining the dynamics of RNAs are not yet widely applied. One promising method for monitoring global dynamics in RNAs involves analysis of RDC data. With the assumption of a motional model, the amplitude of motion of two separate domains can be determined from the differences in the alignment tensors determined from RDC data. This global information can be complemented with information on local dynamics obtained from NMR relaxation experiments. The timescale and/or amplitude of conformational fluctuations can be modeled from relaxation experiments that probe dipole–dipole, cross-correlation, or chemical-exchange processes. Combined with specific-labeling approaches, these methods have enormous potential for monitoring the motion of individual nucleotides on the ps to ms timescale. Application of these methods should permit studies of conformational motions at timescales approaching the rates for some RNA folding and catalytic processes. Taken together, these recent advances in NMR methodologies are providing a wealth of new biochemical information that will dramatically increase our understanding of RNA structure, dynamics, and function.

Acknowledgements

This work was supported in part by the National Institutes of Health (Grant nos.: AI33098 and AI30726) and the NMR instrumentation was purchased with partial support from the National Institutes of Health (Grant no.: RR11969) and the National Science Foundation (Grant no.: 9602941). M.P.L. was supported in part by a National Institutes of Health Training Grant (Grant no.: GM65103). We also thank the W. M. Keck Foundation for their generous support of RNA research on the Boulder campus.

Keywords: conformational dynamics · isotopic labeling · NMR spectroscopy · ribozymes · RNA structures

[1] L. Zidek, R. Stefl, V. Sklenár, *Curr. Opin. Struct. Biol.* **2001**, *11*, 275 – 281.
[2] B. Fürtig, C. Richter, J. Wöhnert, H. Schwalbe, *ChemBioChem* **2003**, *4*, 936 – 962.
[3] J. F. Milligan, D. R. Groebe, G. W. Witherell, O. C. Uhlenbeck, *Nucleic Acids Res.* **1987**, *15*, 8783 – 8789.
[4] C. Kao, S. Rudisser, M. X. Zheng, *Methods* **2001**, *23*, 201 – 205.
[5] J. Lapham, D. M. Crothers, *RNA* **1996**, *2*, 289 – 296.
[6] C. A. Grosshans, T. R. Cech, *Nucleic Acids Res.* **1991**, *19*, 3875 – 3880.
[7] A. R. Ferre-D'Amare, J. A. Doudna, *Nucleic Acids Res.* **1996**, *24*, 977 – 978.
[8] T. P. Shields, E. Mollova, L. S. Marie, M. R. Hansen, A. Pardi, *RNA* **1999**, *5*, 1259 – 1267.
[9] E. P. Nikonowicz, A. Sirr, P. Legault, F. M. Jucker, L. M. Baer, A. Pardi, *Nucleic Acids Res.* **1992**, *20*, 4507 – 4513.
[10] R. D. Batey, M. Inada, E. Kujawinski, J. D. Puglisi, J. R. Williamson, *Nucleic Acids Res.* **1992**, *20*, 4515 – 4523.
[11] R. T. Batey, J. L. Battiste, J. R. Williamson, *Methods Enzymol.* **1995**, *261*, 300 – 322.
[12] D. Yue, PhD Thesis, Iowa State University, Ames, IA, **1994**.
[13] C. Tisne, M. Rigourd, R. Marquet, C. Ehresmann, F. Dardel, *RNA* **2000**, *6*, 1403 – 1412.
[14] A. Vermeulen, S. A. McCallum, A. Pardi, *Biochemistry* **2005**, *44*, 6024 – 6033.
[15] E. P. Nikonowicz, M. Michnicka, K. Kalurachchi, E. DeJong, *Nucleic Acids Res.* **1997**, *25*, 1390 – 1396.
[16] E. P. Nikonowicz, K. Kalurachchi, E. DeJong, *FEBS Lett.* **1997**, *415*, 109 – 113.
[17] L. G. Scott, T. J. Tolbert, J. R. Williamson, *RNA–Ligand Interact. Part A* **2000**, *317*, 18 – 38.
[18] D. W. Hoffman, J. A. Holland, *Nucleic Acids Res.* **1995**, *23*, 3361 – 3362.
[19] I. Kim, P. J. Lukavsky, J. D. Puglisi, *J. Am. Chem. Soc.* **2002**, *124*, 9338 – 9339.
[20] P. J. Romaniuk, O. C. Uhlenbeck, *Methods Enzymol.* **1983**, *100*, 52 – 59.
[21] F. E. Wincott, N. Usman in *Methods in Molecular Biology, Vol. 74*: Ribozyme Protocols *(Ed.: P. C. Turner), Humana Press, Totowa, NJ, **1997**, pp. 59 – 68.*
[22] P. J. Lukavsky, J. D. Puglisi, *RNA* **2004**, *10*, 889 – 893.
[23] J. S. Kieft, R. T. Batey, *RNA* **2004**, *10*, 988 – 995.
[24] K. Pervushin, A. Ono, C. Fernandez, T. Szyperski, M. Kainosho, K. Wüthrich, *Proc. Natl. Acad. Sci. USA* **1998**, *95*, 14147 – 14151.
[25] A. J. Dingley, S. Grzesiek, *J. Am. Chem. Soc.* **1998**, *120*, 8293 – 8297.
[26] A. J. Dingley, J. E. Masse, R. D. Peterson, M. Barfield, J. Feigon, S. Grzesiek, *J. Am. Chem. Soc.* **1999**, *121*, 6019 – 6027.
[27] A. J. Dingley, J. E. Masse, J. Feigon, S. Grzesiek, *J. Biomol. NMR* **2000**, *16*, 279 – 289.
[28] A. Majumdar, Y. Gosser, D. J. Patel, *J. Biomol. NMR* **2001**, *21*, 289 – 306.
[29] J. Wohnert, A. J. Dingley, M. Stoldt, M. Gorlach, S. Grzesiek, L. R. Brown, *Nucleic Acids Res.* **1999**, *27*, 3104 – 3110.
[30] M. Barfield, A. J. Dingley, J. Feigon, S. Grzesiek, *J. Am. Chem. Soc.* **2001**, *123*, 4014 – 4022.
[31] D. Bytchenkoff, E. Chiarparin, D. Fruh, S. Rudisser, G. Bodenhausen, *Magn. Reson. Chem.* **2002**, *40*, 377 – 379.
[32] B. Luy, U. Richter, E. S. DeJong, O. W. Sorensen, J. P. Marino, *J. Biomol. NMR* **2002**, *24*, 133 – 142.
[33] S. Grzesiek, F. Cordier, V. Jaravine, M. Barfield, *Prog. Nucl. Magn. Reson. Spectrosc.* **2004**, *45*, 275 – 300.
[34] A. Z. Liu, A. Majumdar, W. D. Hu, A. Kettani, E. Skripkin, D. J. Patel, *J. Am. Chem. Soc.* **2000**, *122*, 3206 – 3210.
[35] M. Hennig, J. R. Williamson, *Nucleic Acids Res.* **2000**, *28*, 1585 – 1593.
[36] J. Wohnert, A. J. Dingley, M. Stoldt, M. Gorlach, S. Grzesiek, L. R. Brown, *Nucleic Acids Res.* **1999**, *27*, 3104 – 3110.
[37] D. G. Sashital, G. Cornilescu, S. E. Butcher, *Nat. Struct. Mol. Biol.* **2004**, *11*, 1237 – 1242.
[38] J. Noeske, C. Richter, M. A. Grundl, H. R. Nasiri, H. Schwalbe, J. Wohnert, *Proc. Natl. Acad. Sci. USA* **2005**, *102*, 1372 – 1377.
[39] A. Vermeulen, H. Zhao, A. Pardi, *J. Am. Chem. Soc.* **2000**, *122*, 9638 – 9647.

[40] N. Tjandra, A. Bax, *Science* **1997**, *278*, 1111 – 1114.
[41] M. R. Hansen, L. Mueller, A. Pardi, *Nat. Struct. Biol.* **1998**, *5*, 1065 – 1074.
[42] A. Bax, G. Kontaxis, N. Tjandra, *Methods Enzymol.* **2001**, *339*, 127 – 174.
[43] R. Lavery, H. Sklenar, *J. Biomol. Struct. Dyn.* **1989**, *6*, 655 – 667.
[44] L. Zidek, H. H. Wu, J. Feigon, V. Sklenár, *J. Biomol. NMR* **2001**, *21*, 153 – 160.
[45] J. Boisbouvier, D. L. Bryce, E. O'Neil-Cabello, E. P. Nikonowicz, A. Bax, *J. Biomol. NMR* **2004**, *30*, 287 – 301.
[46] J. L. Yan, T. Corpora, P. Pradhan, J. H. Bushweller, *J. Biomol. NMR* **2002**, *22*, 9 – 20.
[47] B. Fürtig, C. Richter, W. Bermel, H. Schwalbe, *J. Biomol. NMR* **2004**, *28*, 69 – 79.
[48] R. Fiala, M. L. Munzarova, V. Sklenár, *J. Biomol. NMR* **2004**, *29*, 477 – 490.
[49] E. Miclet, E. O'Neil-Cabello, E. P. Nikonowicz, D. Live, A. Bax, *J. Am. Chem. Soc.* **2003**, *125*, 15 740 – 15 741.
[50] E. O'Neil-Cabello, D. L. Bryce, E. P. Nikonowicz, A. Bax, *J. Am. Chem. Soc.* **2004**, *126*, 66 – 67.
[51] P. Vallurupalli, P. B. Moore, *J. Biomol. NMR* **2002**, *24*, 63 – 66.
[52] M. Ottiger, F. Delaglio, A. Bax, *J. Magn. Reson.* **1998**, *131*, 373 – 378.
[53] E. O'Neil-Cabello, Z. G. Wu, D. L. Bryce, E. P. Nikonowicz, A. Bax, *J. Biomol. NMR* **2004**, *30*, 61 – 70.
[54] M. R. Hansen, M. Rance, A. Pardi, *J. Am. Chem. Soc.* **1998**, *120*, 11 210 – 11 211.
[55] J. Boisbouvier, F. Delaglio, A. Bax, *Proc. Natl. Acad. Sci. USA* **2003**, *100*, 11 333 – 11 338.
[56] E. T. Mollova, M. R. Hansen, A. Pardi, *J. Am. Chem. Soc.* **2000**, *122*, 11 561 – 11 562.
[57] K. Bondensgaard, E. T. Mollova, A. Pardi, *Biochemistry* **2002**, *41*, 11 532 – 11 542.
[58] M. Zweckstetter, A. Bax, *J. Biomol. NMR* **2002**, *23*, 127 – 137.
[59] R. Bruschweiler, X. B. Liao, P. E. Wright, *Science* **1995**, *268*, 886 – 889.
[60] P. J. Lukavsky, I. Kim, G. A. Otto, J. D. Puglisi, *Nat. Struct. Biol.* **2003**, *10*, 1033 – 1038.
[61] J. R. Tolman, J. M. Flanagan, M. A. Kennedy, J. H. Prestegard, *Proc. Natl. Acad. Sci. USA* **1995**, *92*, 9279 – 9283.
[62] D. L. Bryce, J. Boisbouvier, A. Bax, *J. Am. Chem. Soc.* **2004**, *126*, 10 820 – 10 821.
[63] Q. Zhang, R. Throolin, S. W. Pitt, A. Serganov, H. M. Al-Hashimi, *J. Am. Chem. Soc.* **2003**, *125*, 10 530 – 10 531.
[64] H. M. Al-Hashimi, H. Valafar, M. Terrell, E. R. Zartler, M. K. Eidsness, J. H. Prestegard, *J. Magn. Reson.* **2000**, *143*, 402 – 406.
[65] R. D. Beger, V. M. Marathias, B. F. Volkman, P. H. Bolton, *J. Magn. Reson.* **1998**, *135*, 256 – 259.
[66] A. Dvoretsky, V. Gaponenko, P. R. Rosevear, *FEBS Lett.* **2002**, *528*, 189 – 192.
[67] J. R. Tolman, J. M. Flanagan, M. A. Kennedy, J. H. Prestegard, *Nat. Struct. Biol.* **1997**, *4*, 292 – 297.
[68] Z. Wu, F. Delaglio, N. Tjandra, V. B. Zhurkin, A. Bax, *J. Biomol. NMR* **2003**, *26*, 297 – 315.
[69] H. M. Al-Hashimi, Y. Gosser, A. Gorin, W. D. Hu, A. Majumdar, D. J. Patel, *J. Mol. Biol.* **2002**, *315*, 95 – 102.
[70] H. M. Al-Hashimi, S. W. Pitt, A. Majumdar, W. J. Xu, D. J. Patel, *J. Mol. Biol.* **2003**, *329*, 867 – 873.
[71] J. R. Tolman, H. M. Al-Hashimi, L. E. Kay, J. H. Prestegard, *J. Am. Chem. Soc.* **2001**, *123*, 1416 – 1424.
[72] M. Guéron, J. L. Leroy, *Methods Enzymol.* **1995**, *261*, 383 – 413.
[73] J. Boisbouvier, B. Brutscher, A. Pardi, D. Marion, J. P. Simorre, *J. Am. Chem. Soc.* **2000**, *122*, 6779 – 6780.
[74] N. J. Reiter, H. Blad, F. Abildgaard, S. E. Butcher, *Biochemistry* **2004**, *43*, 13 739 – 13 747.
[75] M. Akke, R. Fiala, F. Jiang, D. Patel, A. G. Palmer, *RNA* **1997**, *3*, 702 – 709.
[76] C. G. Hoogstraten, J. R. Wank, A. Pardi, *Biochemistry* **2000**, *39*, 9951 – 9958.
[77] F. Gaudin, L. Chanteloup, N. T. Thuong, G. Lancelot, *Magn. Reson. Chem.* **1997**, *35*, 561 – 565.
[78] T. Yamazaki, R. Muhandiram, L. E. Kay, *J. Am. Chem. Soc.* **1994**, *116*, 8266 – 8278.
[79] A. G. Palmer, C. D. Kroenke, J. P. Loria, *Methods Enzymol.* **2001**, *339*, 204 – 238.
[80] C. Deverell, R. E. Morgan, J. H. Strange, *Mol. Phys.* **1970**, *18*, 553 – 559.
[81] J. E. Wedekind, D. B. McKay, *Annu. Rev. Biophys. Bioeng.* **1998**, *27*, 475 – 502.
[82] K. Bondensgaard, E. T. Mollova, A. Pardi, *Biochemistry* **2002**, *41*, 11 532 – 11 542.
[83] C. G. Hoogstraten, J. R. Wank, A. Pardi, *Biochemistry* **2000**, *39*, 9951 – 9958.
[84] K. T. Dayie, A. S. Brodsky, J. R. Williamson, *J. Mol. Biol.* **2002**, *317*, 263 – 278.
[85] D. G. Davis, M. E. Perlman, R. E. London, *J. Magn. Reson. Ser. B* **1994**, *104*, 266 – 275.
[86] G. S. Bassi, A. I. H. Murchie, F. Walter, R. M. Clegg, D. M. J. Lilley, *EMBO J.* **1997**, *16*, 7481 – 7489.
[87] A. Khvorova, A. Lescoute, E. Westhof, S. D. Jayasena, *Nat. Struct. Biol.* **2003**, *10*, 708 – 712.
[88] M. D. Canny, F. M. Jucker, E. Kellogg, A. Khvorova, S. D. Jayasena, A. Pardi, *J. Am. Chem. Soc.* **2004**, *126*, 10 848 – 10 849.
[89] E. P. Nikonowicz, A. Pardi, *Nature* **1992**, *355*, 184 – 186.
[90] O. C. Uhlenbeck, *RNA* **1995**, *1*, 4 – 6.
[91] F. Delaglio, S. Grzesiek, G. W. Vuister, G. Zhu, J. Pfeifer, A. Bax, *J. Biomol. NMR* **1995**, *6*, 277 – 293.
[92] T. D. Goddard, D. G. Kneller, SPARKY3, University of California, San Francisco, CA, http://www.cgl.ucsf.edu/home/sparky.

Received: March 28, 2005

